8.A.6 Nuclear Physics B33 (1971) 221–238. North-Holland Publishing Company

TWO HIGH ENERGY PROCESSES INVOLVING DETECTED FINAL STATE PARTICLES

P.V.LANDSHOFF and J.C.POLKINGHORNE
Department of Applied Mathematics and Theoretical Physics, University of Cambridge, England

Received 29 March 1971
(Revised 16 June 1971)

Abstract: Two processes are discussed: (a) semi-inclusive electroproduction experiments; (b) heavy-lepton pair production in hadronic collisions. The non-perturbative approach to the parton model is used to evaluate scaling properties and to consider extra contributions due to wee partons. These latter have not been previously discussed and are found to be important for process (b), but absent in process (a). Quantitative agreement is obtained for process (b), including an explanation of the observed shoulder in the differential cross section.

1. INTRODUCTION

In a recent paper [1] we have given a general formulation of the parton model, using a non-perturbative field theory approach. We then combined this with notions of duality, to give a description of deep inelastic electron or neutrino reactions based on the identification of partons with quarks [2].

This discussion was concerned with inclusive experiments, where none of the hadrons in the final state is detected. In this paper we use the same parton model to consider the corresponding semi-inclusive processes:

$$\ell + h \to \ell' + h' + H , \tag{1.1}$$

where ℓ is a lepton, h and h′ are definite hadrons and H is an undetected system of hadrons (fig. 1). We also consider heavy lepton pair production:

$$h + h' \to \ell + \bar{\ell} + H , \tag{1.2}$$

where again the final state hadrons are not detected (fig. 2). Both processes (1.1) and (1.2) have previously been discussed by Drell and Yan [3,4] using their perturbation theory approach to the parton model. However they were not able to discuss

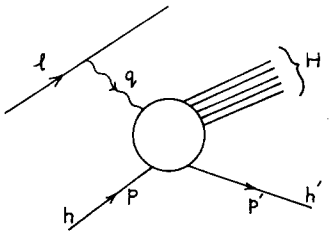

Fig. 1. The semi-inclusive electroproduction process.

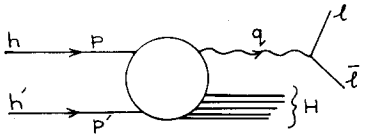

Fig. 2. The heavy-lepton-pair production process.

certain hadronic effects. These are effects associated with partons that have a very small fraction of the longitudinal momentum of their parent hadron. Feynman [5] has emphasised the importance of the exchange of these "wee" partons in generating constant total cross sections.

We shall find (sect. 4) that pomeron exchange makes an important contribution to the reaction (1.2), though not to (1.1). We reach this conclusion without making any detailed assumption about the nature of the pomeron or how it is generated. We intend to discuss these latter topics in a further paper [6].

In sects. 2 and 3 we consider contributions to the processes (1.1) and (1.2) that are independent of these effects. We confirm the scaling laws already obtained by Drell and Yan [3,4]. However we do not agree with a detailed result of a factored form for (1.1) which they obtain. Also we obtain the additional diffractive contribution to (1.2) already referred to. This term is of the same order in the energy variable s except perhaps for a function of $\log s$. The presence of factors of $\log s$ is, of course, unlikely to be significant at physically accessible values of s.

In sect. 5 we discuss the comparison of our theory with data for heavy-muon pair production. Good quantitative agreement is obtained. The diffractive term is found to dominate for small values of q^2 while the term of the type found by Drell and Yan (but modified in magnitude because of our different understanding of the role of anti-partons) is important for larger values of q^2. The shoulder in the plot of $\mathrm{d}\sigma/\mathrm{d}\sqrt{q^2}$ against q^2 results from the change over between these two contributions.

2. SEMI-INCLUSIVE PROCESSES

Consider processes of the type (1.1), where a sum is taken over possible constituents of the system H and over the polarisations of the hadron h′, with an average over the polarisations of h. Label the momenta as in fig. 1. Following Drell and Yan [3], we consider the momentum p' of the final hadron h′ as being constrained by assigning values to the scalar products

$$\nu' = p' \cdot q \,, \qquad \kappa = p' \cdot p \,. \tag{2.1}$$

Together with $p'^2 = M'^2$, these relations determine p' to within an angle, which will be integrated over. We write

$$\frac{1}{2\pi}\int \mathrm{d}^4p'\,\delta^{(+)}(p'^2 - M'^2)\delta(p'\cdot q - \nu)\delta(p'\cdot p - \kappa)\,.$$

$$\times \sum_{\mathrm{H}} \langle p|j_\mu(0)|p',\mathrm{H}\rangle\langle p',\mathrm{H}|j_\nu(0)|p\rangle$$

$$= -\left(g_{\mu\nu} - \frac{q_\mu q_\nu}{q^2}\right)\mathcal{W}_1 + \frac{1}{M^2}\left(p_\mu - \frac{p\cdot q}{q^2}\,q_\mu\right)\left(p_\nu - \frac{p\cdot q}{q^2}\,q_\nu\right)\mathcal{W}_2\,. \tag{2.2}$$

The structure functions $\mathcal{W}_1$ and $\mathcal{W}_2$ are functions of $q^2, \nu = p\cdot q, \nu'$ and κ. The matrix element (2.2) is related, in a not altogether simple way, to the (connected) amplitude drawn in fig. 3a. The vertical line indicates that the amplitude must be "cut" in the channel indicated, that is a complete set of physical intermediate states H must be inserted. The (+) sign indicates that the energy variables to the left of this cut must be evaluated from the physical limit; the (−) sign requires the energy variables to the right of the cut to approach their real values from the complex conjugate limit.

According to the parton picture formulated in ref. [1], the current interacts directly with a parton field, so that fig. 3a is equivalent to fig. 3b, where the broken lines denote this parton field. If there are several different types of parton, as in the quark model [2], a sum over parton types is understood. In the usual way, it is supposed that the four-parton/four-hadron amplitude contained within fig. 3b has disconnected parts. The contributions from these are drawn in fig. 4; there are two terms of each type, related to each other by the replacement (parton ↔ anti-parton). In fig. 4a the upper bubble represents a complete parton propagator; the other bubbles in fig. 4 are non-amputated amplitudes, that is it is not necessary to include separate propagators for the parton lines attached to them.

In this section we analyse the contributions from fig. 4. The possibility that there is also an important contribution from the connected part of the amplitude within fig. 3b is disposed of in sect. 4.

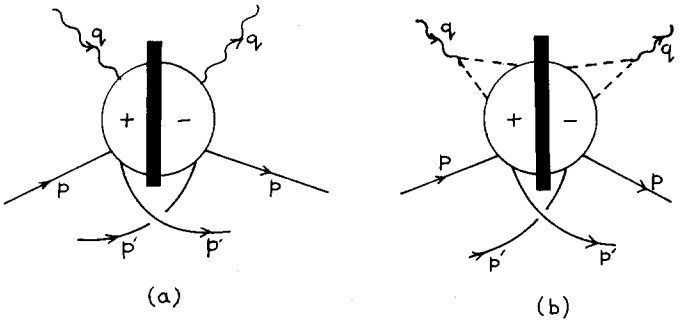

Fig. 3. Contributions relevant to the process of fig. 1.

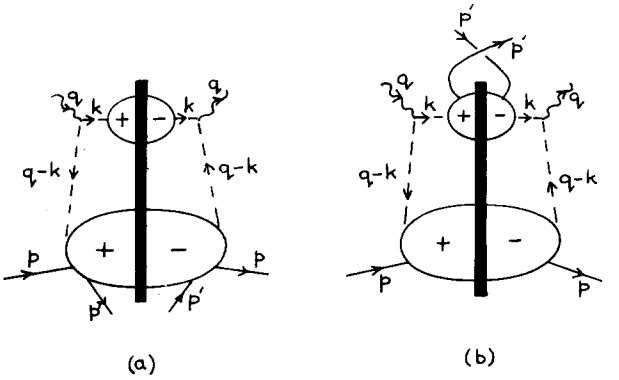

Fig. 4. Those parts of the contributions of fig. 3 which are independent of wee parton effects.

Define

$$\omega = -\frac{2\nu}{q^2}, \qquad u = \frac{\nu'}{\nu}, \qquad \eta = \frac{\kappa}{\nu}. \tag{2.3}$$

We investigate the limit in which $\nu \to \infty$, with ω, u and η remaining bounded. Write

$$p' = \alpha p + \beta q + \chi, \tag{2.4}$$

where the momentum χ is defined to be orthogonal to both p and q and so is space-like, $\chi^2 \leqslant 0$. The condition $p'^2 = M'^2$ and the definitions (2.3) give, as $\nu \to \infty$,

$$\beta\left(\alpha-\frac{\beta}{\omega}\right)=O\left(\frac{1}{\nu}\right),$$

$$u-\alpha+\frac{2\beta}{\omega}=O\left(\frac{1}{\nu}\right), \tag{2.5}$$

$$\eta-\beta=O\left(\frac{1}{\nu}\right).$$

(We assume that α, β and κ^2 remain bounded as $\nu \to \infty$; cf. the appendix of ref. [1].) The first condition in (2.5) has two extreme solutions:

either $$\beta = O\left(\frac{1}{\nu}\right), \quad \text{i.e.} \quad \eta \to 0\ , \tag{2.6a}$$

or $$\alpha-\frac{\beta}{\omega}=O\left(\frac{1}{\nu}\right), \quad \text{i.e.} \quad u \to -\frac{\eta}{\omega}\ . \tag{2.6b}$$

We shall find that these correspond to figs. 4a and 4b respectively. The class of intermediate solutions, where both β and $(\alpha-\beta/\omega)\to 0$ in such a way that their product is $O(1/\nu)$, is discussed in sect. 4.

To analyse either diagram in fig. 4, write

$$k = xp + yq + \kappa \tag{2.7}$$

where κ is orthogonal to both p and q. Again, as in ref. [1], the dominant contributions arise from the regions of k-integration where x, y and κ^2 remain bounded as $\nu \to \infty$. Also, as explained in ref. [1], the masses of the parton lines attached to the lower bubble, and its energy variable $s' = (p-k+q)^2$ remain bounded. (The condition on the masses of the parton lines is the basic dynamical postulate of ref. [1], that is it is supposed that the parton field is defined such that the amplitudes concerned go to zero rapidly as the virtual parton mass becomes large. The condition on the energy variable corresponds to the arguments in the appendix of ref. [1].) Thus

$$\left(x-\frac{y-1}{\omega}\right)(y-1)=O\left(\frac{1}{\nu}\right),$$

$$\left(x-1-\frac{y-1}{\omega}\right)(y-1)=O\left(\frac{1}{\nu}\right),$$

and so

$$y-1=O\left(\frac{1}{\nu}\right). \tag{2.8}$$

For fig. 4a there is the additional constraint that the other variable $p' \cdot p$ of the lower bubble remains bounded, as the hadronic amplitude is supposed to go to zero quite rapidly when one of its momentum transfers becomes large. This picks out the solution (2.6a). The calculation for fig. 4a is almost identical with that in ref. [1], except for the complication associated with the (+) and (−) signs on the bubbles, and the extra integration over p'. These new features will be sufficiently illustrated by our discussion of fig. 4b, and so we just give the results for fig. 4a:

$$M^2\nu^2\mathcal{W}_1 \to \delta(\eta)\,\mathcal{F}_1(\omega,u)\,,$$

$$\nu^3\mathcal{W}_2 \to \delta(\eta)\,\mathcal{F}_2(\omega,u)\,,$$

where the functions $\mathcal{F}_1$, $\mathcal{F}_2$ are certain integrals over the two-parton/four-hadron amplitude. They satisfy

$$\begin{aligned} &\mathcal{F}_1 = \tfrac{1}{2}\omega\,\mathcal{F}_2 \qquad \text{for spin-}\tfrac{1}{2}\text{ partons}\,, \\ &\mathcal{F}_1 = 0 \qquad\qquad\quad \text{for scalar partons}\,. \end{aligned} \tag{2.9b}$$

In the case of fig. 4b the energy variable $(k-p')^2$ of the upper bubble has to remain bounded, and also the masses k^2 of the parton lines attached to it. The latter condition is

$$x - \frac{y}{\omega} = \mathrm{O}\left(\frac{1}{\nu}\right), \tag{2.10}$$

and then the former condition picks out the solution (2.6b). Because of (2.6b), (2.8) and (2.10) we change to new variables:

$$\alpha = \frac{\beta}{\omega} + \frac{\bar{\alpha}}{2\nu}\,, \tag{2.11a}$$

$$\begin{aligned} y &= 1 + \frac{\bar{y}}{2\nu}\,, \\ x &= \frac{y}{\omega} + \frac{\bar{x}}{2\nu}\,, \end{aligned} \tag{2.11b}$$

and make the mathematical assumption that we may take the limit $\nu \to \infty$ under the integral. In this limit

$$\mathrm{d}^4k \to \frac{1}{4\nu}\,\mathrm{d}\bar{x}\mathrm{d}\bar{y}\mathrm{d}^2\kappa\,,$$

$$\mathrm{d}^4p'\delta^{(+)}(p'^2-M'^2)\delta(p'\cdot q-\nu')\delta(p'\cdot p-\kappa)$$

$$\to \frac{1}{2\nu^2}\,\mathrm{d}\bar{\alpha}\mathrm{d}\bar{\beta}\mathrm{d}^2\chi\theta(\beta)\delta(u^2M^2+\chi^2+\eta\bar{\alpha}-M'^2)$$

$$\times\,\delta\left(u+\frac{\beta}{\omega}\right)\delta(\eta-\beta)\,. \tag{2.12}$$

The energy variable of the lower bubble is

$$(p+q-k)^2 = \bar{y}\left(\frac{1}{\omega}-1\right)+\left(\frac{1}{\omega}-1\right)^2 M^2+\kappa^2\,. \tag{2.13a}$$

We have to insert a complete set of intermediate states in this variable, taking the (+) limit for the left-hand part of the resulting expression and the (−) limit for the right-hand part. The mass variable associated with this bubble is

$$(k-q)^2 = \frac{\bar{y}}{\omega}+\frac{M^2}{\omega^2}+\kappa^2\,. \tag{2.13b}$$

If we remember that κ is spacelike, $\kappa^2 \leqslant 0$, and that $\omega > 1$, we find that $(k-q)^2$ is negative for the values of (2.13a) above threshold to which the integration is restricted. Hence throughout the integration we are clear of the branch-cuts in the variable (2.13b), and the presence of these cuts does not have to be taken into account in the (±) prescriptions. That is, so far as the lower amplitude is concerned, by unitarity, the integration is simply over its imaginary part.

For the upper amplitude the situation is more complicated. The insertion of intermediate states is in the variable

$$(k-p')^2 = (1-\eta)(\bar{x}-\bar{\alpha})+(1-\eta)^2\frac{M^2}{\omega^2}+(\kappa-\chi)^2\,. \tag{2.14a}$$

But the mass variable

$$k^2 = \bar{x}+\frac{M^2}{\omega^2}+\kappa^2\,, \tag{2.14b}$$

has to support these intermediate states together with p', and so is also above threshold. In the left-hand part of the amplitude the integration contour is on the upper side of the k^2 branch-cut; in the right-hand part it is on the lower side. Unitarity tells us nothing about this; the unitarity relation involves terms with intermediate states in the k^2 variable in addition to the term we want that has intermediate states in the variable (2.14a). All we can say is that, because of our postulate that the amplitude becomes small as k^2 becomes large, we expect that the integral will converge.

If we take into account the way the current couples to the partons, and handle the complication of spin-$\frac{1}{2}$ partons by methods similar to those described in ref. [1], we finally obtain asymptotic contributions

$$\begin{aligned} M^2\nu^2 \mathcal{W}_1 &\to \delta\left(u+\frac{\eta}{\omega}\right)\bar{\mathcal{F}}_1(\omega,u)\,, \\ \nu^3 \mathcal{W}_2 &\to \delta\left(u+\frac{\eta}{\omega}\right)\bar{\mathcal{F}}_2(\omega,u)\,, \end{aligned} \tag{2.15}$$

where the functions $\bar{\mathcal{F}}_1$, $\bar{\mathcal{F}}_2$ obey relations exactly similar to (2.9b). Unlike Drell and Yan [2], we do not find that these functions have any simple factorisation properties; for example, the presence of the integration variable κ in (2.14a) prevents us from extracting a factor $F_2(\omega)$ from $\bar{\mathcal{F}}_2(\omega,u)$.

We take this opportunity to mention that in our discussion in ref. [1] of the deep annihilation process we encountered a situation similar to that described above, where the integration region is enclosed by cuts in the mass variable. We speculated that the pinches between the ($\pm$) singularities in the mass variables might cause a divergence of the integral, corresponding to enhanced scaling properties. Such a divergence has actually been encountered in a Veneziano-like amplitude [7]. It would certainly occur in parton models if the pinching singularities were poles. However, if the quarks are not asymptotically observable particles there are no poles and in any case the poles would, for kinematic reasons, not occur on the integration contour. Thus we now incline to the view that the functions $\bar{W}_1$ and $\nu\bar{W}_2$ of deep annihilation do scale (though they almost certainly cannot be obtained by a simple analytic continuation of the electroproduction functions F_1 and F_2), and the divergence found in the Veneziano model is perhaps a reflection of the narrow-resonance approximation of that model.

3. HEAVY LEPTON PAIR PRODUCTION

Consider now the reaction (1.2), with the momenta labelled as in fig. 2 and where averages over the polarisations of h and h′ are understood. We are interested in the kinematic region where

$$\begin{aligned} &s = (p+p')^2 \to \infty\,, \\ &\tau = q^2/s \text{ fixed}\,. \end{aligned} \tag{3.1}$$

The cross section $\mathrm{d}\sigma/\mathrm{d}q^2$ is obtained from the structure function [4]

$$W(s,\tau) = \int \mathrm{d}^4q\,\delta^{(+)}(q^2-\tau s)\int \mathrm{d}^4x\, \mathrm{e}^{-iqx}\,\langle p,p'|J_\mu(x)J^\mu(0)|p,p'\rangle\,. \tag{3.2}$$

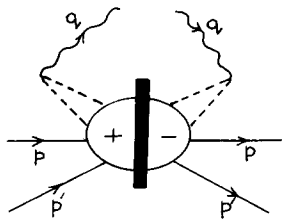

Fig. 5. Contributions relevant to the process of fig. 2.

We couple the current to the parton field as before, so that (3.2) corresponds to the (connected) amplitude drawn as in fig. 5, cut in the manner indicated. Again, W is not the imaginary part of the two-current amplitude; the unitarity equation that gives the imaginary part contains extra terms, which we do not want. The "cut" denoted by the vertical line in fig. 5 represents insertion of a complete set of intermediate states H, with the parts of the diagram to either side of the cut evaluated in complex-conjugate limits.

The four-parton/four-hadron amplitude contains disconnected parts. If we insert these in fig. 5, one of the resulting terms is as drawn in fig. 6. The others may be shown to be of lower order in s as $s \to \infty$. In sect. 4 we show that a part of the connected amplitude contributes to fig. 5 a contribution of the same order in s as fig. 6, to within a possible function of $\log s$. This is the pomeron exchange contribution of fig. 7 (the zigzag line represents the pomeron).

In this section we consider fig. 6. Write

$$k_i = x_i p + y_i p' + \kappa_i , \qquad i = 1, 2 , \tag{3.3}$$

where the κ_i are orthogonal to p and p', so that they are spacelike, $\kappa_i^2 \leqslant 0$. As explained in the paragraph preceding (2.8), we require the parton masses k_1^2, k_2^2 and the energy variables of the internal amplitudes to remain bounded as $s \to \infty$. This results in

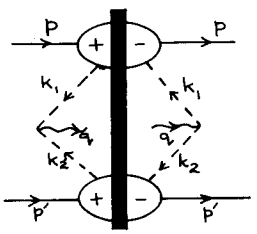

Fig. 6. Those parts of the contributions of fig. 5 which are independent of wee parton effects.

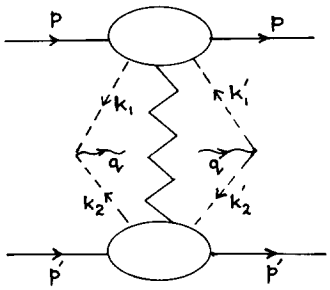

Fig. 7. Possible pomeron-exchange contributions to fig. 5.

$$y_1 = \bar{y}_1/s\,, \qquad x_2 = \bar{x}_2/s\,, \tag{3.4}$$

where $\bar{y}_1, \bar{x}_2$ are bounded. Then

$$\int \mathrm{d}^4q\,\mathrm{d}^4k_1\,\mathrm{d}^4k_2\,\delta^{(4)}(k_1+k_2-q)\,\delta^{(+)}(q^2-\tau s)$$

$$\to \frac{1}{4s}\int \mathrm{d}x_1\,\mathrm{d}\bar{y}_1\,\mathrm{d}\bar{x}_2\,\mathrm{d}y_2\,\mathrm{d}^2\kappa_1\,\mathrm{d}^2\kappa_2\,\delta(x_1y_2-\tau)\,\theta(x_1+y_2)\,, \tag{3.5}$$

and

$$(p-k_1)^2 \sim (x_1-1)\bar{y}_1 + (x_1-1)^2\,M^2 + \kappa_1^2\,. \tag{3.6}$$

When we make the required cut in fig. 6, the energy variable (3.6) has to be above the threshold for the upper amplitude and $p^0 - k_1^0$ has to be positive. Hence we find, using also (3.5),

$$0 \leqslant x_1 \leqslant 1\,. \tag{3.7}$$

This means that the mass variable of the upper bubble,

$$k_1^2 \sim x_1\bar{y}_1 + x_1^2M^2 + \kappa_1^2 \tag{3.8}$$

is negative and away from its branch cut. So as explained in sect. 2, making the required cut in the upper amplitude is equivalent to taking its imaginary part. The same applies to the lower amplitude.

Taking account of the appropriate coupling of the currents to the partons, we obtain a contribution from fig. 9 proportional to

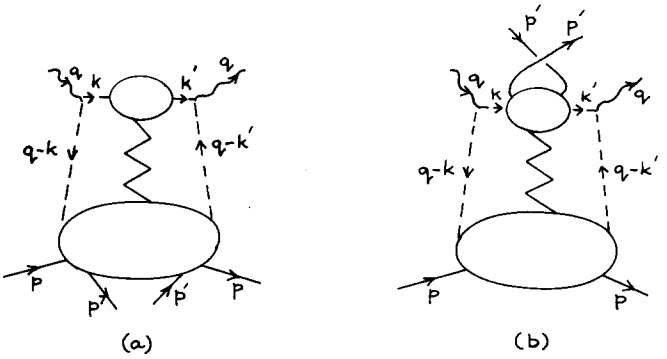

Fig. 8. Possible pomeron-exchange contributions to fig. 3.

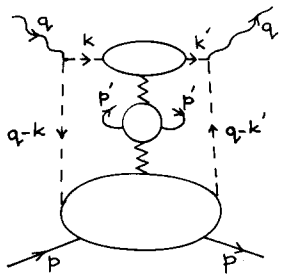

Fig. 9. Further possible pomeron-exchange contributions to fig. 3.

$$\frac{1}{\lambda_a^2 \tau} \int_1^\infty d\omega_1 d\omega_2 \delta\left(\omega_1 \omega_2 - \frac{1}{\tau}\right) F_{2a}(\omega_1) F'_{2\bar{a}}(\omega_2) \,. \tag{3.9}$$

Here λ_a is the charge on the internal parton, F_{2a} is the contribution that the parton makes to the electroproduction structure function F_2 (as calculated in ref. [1]) for hadron h as target, and $F'_{2\bar{a}}$ is the contribution the corresponding antiparton makes for electroproduction with hadron h′ as target. A similar result has been previously obtained by Drell and Yan [4].

4. DIFFRACTIVE EFFECTS

We now consider contributions from the connected parts of the internal ampli-

tudes in figs. 3b and 5. Power counting arguments suggest that the effects of pomeron exchange within these amplitudes are likely to be important.

Consider first the contribution of fig. 7 to heavy-lepton-pair production. Here the zigzag line represents the pomeron. For our present purposes it will not be necessary to consider a detailed picture of how the pomeron is generated. The two bubbles in fig. 7 are pomeron coupling functions; according to usual ideas they go to zero rapidly when any of their mass variables becomes large, in exactly the same way as we have postulated for the bubbles in the other figures, which represent hadronic amplitudes. Thus the kinematics of fig. 7 are very similar to fig. 6. There are two extra momentum variables, but k_1' is constrained like k_1, and k_2' like k_2. Thus [cf. (3.3), (3.4), (3.5)]

$$\int \mathrm{d}^4q \mathrm{d}^4k_1 \mathrm{d}^4k_2 \mathrm{d}^4k_1' \mathrm{d}^4k_2' \delta^{(4)}(k_1+k_2-q)\delta^{(4)}(k_1'+k_2'-q)\delta^{(+)}(q^2-\tau s)$$

$$\to \frac{1}{4s^2} \int \mathrm{d}x_1 \mathrm{d}\bar{y}_1 \mathrm{d}\bar{x}_2 \mathrm{d}y_2 \mathrm{d}x_1' \mathrm{d}\bar{y}_1' \mathrm{d}\bar{x}_2' \mathrm{d}y_2' \mathrm{d}^2\kappa_1 \mathrm{d}^2\kappa_2 \mathrm{d}^2\kappa_1' \mathrm{d}^2\kappa_2'$$

$$\times \delta(x_1-x_1')\delta(y_2-y_2')\delta^{(2)}(\kappa_1+\kappa_2-\kappa_1'-\kappa_2')\, \delta(x_1y_2-\tau)\theta(x_1+y_2)\,. \tag{4.1}$$

Compared with (3.5), there is an extra power of s^{-1}, but this is compensated by an extra power of s arising from the pomeron. There is also expected to be a function of $\log s$, depending on the exact nature of the pomeron singularity. Hence apart from this possible function of $\log s$, the contribution from fig. 7 appears to be of the same order as that from fig. 6.

Notice however that care is needed with this type of power-counting argument. Consider the contribution from fig. 8a to fig. 3b, that is to the reaction (1.1). The kinematics are very similar to those for fig. 4a; both k and k' are now constrained like k for fig. 4a. A count of powers of ν suggests that fig. 8a gives a contribution of the same order as fig. 4a. But now this power of ν actually multiplies an integral that vanishes. To see this, we require the mass variables k^2, k'^2, $(q-k)^2$, $(q-k')^2$ of the pomeron coupling functions to remain bounded as $\nu \to \infty$, and so have (2.8) and (2.10), together with analogous conditions on x', y'. Thus we define new variables $\bar{x}$ and $\bar{y}$ as in (2.11b), and similarly $\bar{x}'$ and $\bar{y}'$. When we take the limit $\nu \to \infty$ under the integral, the only variable in which $\bar{x}$ survives is k^2, as in (2.14b). Similarly $\bar{x}'$ survives only in k'^2. In the usual way, we suppose that the analytic structure of the pomeron coupling function is such that its singularities in k^2 are just below the real axis. Hence on completing the contour of $\bar{x}$ integration with an infinite semicircle in the upper half-plane, we obtain a vanishing integral. The $\bar{x}'$ integration also gives zero, in the same way, except that the k'^2 variable is in the half of the diagram that should have a (−) label, so that the $\bar{x}'$ contour will be completed in the lower half plane. (In fact this argument needs slight elaboration. We have to make a cut in the diagram, and this can be done in more than one way – to the right of the pomeron, to its left, or down the middle of it. When we make the cut to the left of the pom-

eron the variable k^2 is not integrated from $-\infty$ to ∞, and so the $\bar{x}$ integration does not vanish. But the $\bar{x}'$ integration still vanishes.) Analogous arguments also prevent there being a contribution of this type in inclusive electroproduction experiments.

An obvious question is whether the the same cancellation happens for fig. 7, that is whether there the $\bar{y}_1$ integration, for example, gives zero. That it does not can be seen from (3.6), (3.7) and (3.8). When $s \to \infty$ the variable $\bar{y}_1$ survives in the two variables k_1^2 and $(p-k_1)^2$. The singularities in each of these variables are just below the real axis, but because of (3.7) they are on opposite sides of the real axis in the $\bar{y}_1$ plane.

The reason that fig. 7 survives, and not fig. 8a, is that the upper bubble depends on more variables and so has a more complicated analytic structure. One might expect that, for a similar reason, the contribution from fig. 8b should be of the same order as that from fig. 4b. But again this is not so. The kinematics are similar to those for fig. 4b, with k' constrained like k, so we again introduce variables $\bar{x}$, $\bar{y}$ as in (2.11b), with $\bar{x}'$ and $\bar{y}'$ similarly defined. When $\nu \to \infty$ the variable $\bar{x}$ survives only in the variables $(k-p')^2$ and k^2, as given in (2.14). Again the singularities in each of these variables are just below the real axis. But one can show that, in order to support the intermediate states when the necessary cut is made, the kinematics imposes the constraint

$$\eta < 1 \,. \tag{4.2}$$

This means that they are both below the real axis in the $\bar{x}$ plane, and so the $\bar{x}$ integration vanishes. The same applies to the $\bar{x}'$ integration.

The extra pomeron contribution associated with fig. 7 is related to the contribution from fig. 6 in a way that is analogous to the relation between a reggeon-pomeron cut and a Regge pole. The power of s associated with the pomeron in fig. 7 is

$$s^{\alpha_P[(\kappa_1-\kappa_1')^2]} \,, \tag{4.3}$$

which gives when integrated with respect to κ_1 and κ_1' a variable power contribution in the scaling limit. A pomeron which is a moving pole with intercept one would give a contribution which, compared with (3.9), decreases like $(\log s)^{-1}$. This logarithmic decrease would be unlikely to affect the significance of the term at physically accessible energies.

Consider now the solution to the first equation in (2.5) that is intermediate between (2.6a) and (2.6b):

$$\beta = \tfrac{1}{2}\bar{\beta}\nu^{-\gamma} \,,$$

$$\alpha - \frac{\beta}{\omega} = \tfrac{1}{2}\bar{\alpha}\nu^{\gamma-1} \,, \qquad 0 < \gamma < 1 \,, \tag{4.2}$$

where α and β are bounded. We associate this with the two pomeron exchange diagram of fig. 9. The momenta k, k' are constrained as before, and the energy variables associated with the two pomerons are

$$(k-p')^2 \sim -\bar{\alpha}\nu^{\gamma} ,$$
$$(p+q-k-p')^2 \sim -\bar{\beta}\nu^{1-\gamma} . \tag{4.3}$$

The product of these is $O(\nu)$, and so again a power count suggests that the contribution is important. But once again the variables $\bar{x}$ and $\bar{x}'$ survive only in k^2 and k'^2 respectively, and so these integrations give zero.

To sum up, the pomeron exchange contribution (fig. 7) to heavy lepton pair contribution is important, but for the inelastic lepton scattering the pomeron exchange effects are of lower order, and figs. 4a and 4b dominate. Of course the amplitudes contained within these figures also receive contributions from the pomeron, but these only manifest themselves directly for large values of ω (see refs. [1,2]).

Finally we may note that the rather surprising presence of pomeron contributions in some regimes and their absence in others has been checked by calculation of simple Feynman diagrams which appropriately model the situations considered. In these α-space calculations the contributions would arise from pinch configurations [8] and the conditions (3.7) and (4.2) exactly correspond to the conditions that these pinches do or do not trap the contour.

5. COMPARISON WITH EXPERIMENT

The differential cross section for (1.2) in the limit (3.1) is given by [4]

$$\frac{d\sigma}{d\sqrt{q^2}} = \frac{8\pi\alpha^2}{3(q^2)^{\frac{3}{2}}} \tau W(\tau) , \tag{5.1}$$

where $W(\tau)$ is the limit of the structure function $W(s,\tau)$ of (3.2). The DY contribution is given by

$$W_{DY}(\tau) = \frac{1}{\tau} \sum_a \lambda_a^{-2} \int_1^{\infty} d\omega_1 d\omega_2 \delta(\omega_1\omega_2 - \tau^{-1}) F_{2a}(\omega_1) F_{2\bar{a}}(\omega_2) , \tag{5.2}$$

where the sum is over the different partons with charges λ_a, and F_{2a} and $F_{2\bar{a}}$ are the contributions, respectively, of parton a and corresponding anti-parton $\bar{a}$ to the limit of νW_2 in deep inelastic electroproduction off the proton.

In making comprison with experiment, using (5.3), Drell and Yan assumed equal momentum distributions for partons and antipartons within the proton. They find

on this basis that the overall scale of the contribution has to be reduced by a factor of 3 or 4 in comparison with the data if a quark-parton picture is used. They are also unable to explain the pronounced shoulder in the data (see fig. 10).

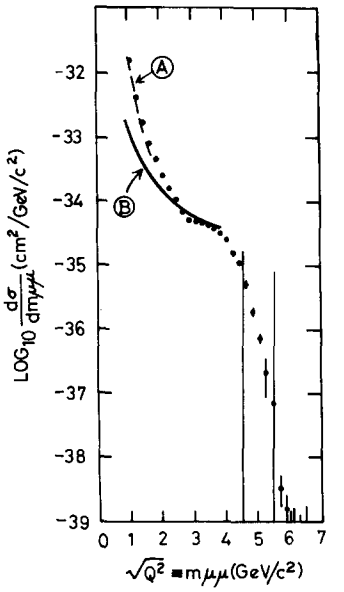

Fig. 10. Comparison with the experimental data: A is the pomeron and B the Drell-Yan term. The two vertical lines contain the region in which sharp fall-off is expected. Notice the log scale.

The dual quark-parton picture [2] does not encourage the idea that anti-quark distributions in the proton are at all comparable to quark distributions. The former are associated only with the diffractive contribution to deep inelastic electroproduction whilst the latter also occur in the (larger) resonance contribution. This resonance contribution may be calculated from the Veneziano-like model previously constructed [10]; the total diffractive contribution is then obtained by subtraction from the experimental data. The diffractive contribution appears to have the character that it is nearly zero for ω less than some value ω_0 lying near 3 and that for values of ω greater than ω_0 it is approximately constant and contributes about 0.13 to the value of νW_2^{eP} [11].

Before comparison can be made with experiment it is necessary to take account of the fact that Christenson et al. impose a cut-off on dimuon laboratory momentum at 12 GeV/c. The incident proton has energy 29.5 GeV and the transverse momentum of the dimuon is sharply limited to less than 1 GeV/c. If the parton comes from the projectile proton and the antiparton from the target proton this corresponds to a cut-off on ω_1 in (5.2) at 2.5.

There is also a term where the role of projectile and target is reversed but in that case the diffractive term, which gives the antiparton, is cut off at $\omega_2 = 2.5$, that is below ω_0, and so this term is negligible.

The sum in (5.2) can thus be performed in the quark parton model to give a DY term

$$\int_1^{2.5} \frac{d\omega}{\omega} R(\omega) D\left(\frac{1}{\tau\omega}\right). \tag{5.3}$$

Here R is the total resonance contribution to νW_2^{eP}, which we calculated from our Veneziano-like model. D is $\frac{3}{4}$ of the total diffractive contribution to νW_2^{eP} and we take for it the form

$$D(\omega) \approx \theta(\omega - \omega_0) \times 0.1 , \tag{5.4}$$

with $\omega_0 \approx 3$. It is not possible to estimate D more accurately at present.

For

$$\tau \geqslant 1/\omega_0 , \tag{5.5}$$

no part of the range in which D is significant contributes to (5.3), and so the non-diffractive contribution is very small when (5.5) holds. The two vertical lines in fig. 10 correspond to (5.5) with $\omega_0 = 3$ and 2 respectively and indicate the region where rapid decrease is expected due to the smallness of the diffractive electroproduction contribution near $\omega = 1$. It is clearly not possible to calculate the details of this fall-off without a more detailed model of the pomeron contribution to electroproduction since the fall is over several decades and so sensitive to very small effects.

If

$$\tau \leqslant \frac{1}{2.5\omega_0} , \tag{5.6}$$

then, assuming (5.4), the factor (5.3) becomes independent of τ and we obtain a contribution to the differential cross section:

$$\frac{d\sigma}{d\sqrt{q^2}} = \frac{1.8 \times 10^{-33}}{(q^2)^{\frac{3}{2}}} \text{ cm}^2/\text{GeV}/c^2 . \tag{5.7}$$

The thick solid curve in fig. 10 represents the contribution (5.7). One sees that it is in good accord with the data in the region $\sqrt{q^2}$ from 2 to 4 GeV/c^2. To the right of this region there is the sharp fall-off we have already explained whose exact shape depends on the precise way in which the diffractive contribution to νW_2^{eP} behaves between $\omega = 1$ and $\omega = 2$ to 3.

We now turn our attention to the region of $\sqrt{q^2}$ less than 2 GeV/c^2 and see if we can explain the higher values of $d\sigma/d\sqrt{q^2}$ which are found there. We shall argue that they are likely to come from the pomeron contribution.

A fully quantitative estimation of the pomeron contribution resulting from (4.1) is not possible without an *ansatz* for the pomeron coupling functions which make up the undisplayed terms in integrand. However we can extract certain features which can be expected to hold for this contribution at small values of τ. Consider the integrations in (4.1). One of our basic assumptions is that the bubbles in fig. 7 are small unless the squared masses on the parton lines are finite. Since, in particular

$$k_2^2 = \bar{x}_2 y_2 + y_2^2 M^2 + \kappa_2^2 ,$$

this constrains the effective range of the integration over $\bar{x}_2$ to values less than $O(y_2^{-1})$. Because of the experimental lower cut-off on q, $x_1 > (2.5)^{-1}$. Thus, because of the $\delta(x_1 y_2 - \tau)$, $y_2 = O(\tau)$ as $\tau \to 0$, and the effective upper limit on $\bar{x}_2$ is $O(\tau^{-1})$. Similar arguments apply to $\bar{x}_2'$. That is, we have

$$\int dx_1 \, d\bar{y}_1 \, d\bar{y}_1' \int^{O(\tau^{-1})} d\bar{x}_2 d\bar{x}_2' , \tag{5.8}$$

with the effective limits on the first three integrations independent of τ. The integrand to which (5.8) is applied contains a factor τ arising from the current couplings. We assume also that the bubbles in fig. 7 behave, for large values of their variables, in the same way as ordinary five-point functions. In particular, when either or both of $(p-k_2)^2$, $(p'+k_2')^2$ is $O(\tau^{-1})$, the lower bubble is supposed to be $O(\tau^{-1})$, corresponding to pomeron exchange. The resulting behaviour of the integral is $O(\tau^{-2})$. As a check, similar arguments give a behaviour $O(\tau^{-1})$ for the Drell-Yan term as $\tau \to 0$.

We cannot say anything quantitative about the factor that multiplies the τ^{-2} in the pomeron term, though we expect it to be not very different from the factor that multiplies τ^{-1} in the DY term. In this case, since in the present experiment, $\tau^{-1} \approx 60$ at $q^2 = 1$, the pomeron term is dominant for τ near to 1. It gives

$$\frac{d\sigma}{d\sqrt{q^2}} \propto \frac{1}{2} \frac{1}{(q^2)^{\frac{3}{2}}} = \frac{s}{(q^2)^{\frac{5}{2}}} , \tag{5.9}$$

so that the differential cross section varies like $(q^2)^{-\frac{5}{2}}$ for small q^2 at fixed s. The broken line in fig. 10 represents a curve with the dependence of (5.9) and normalised to the left-most experimental point in the figure.

It seems therefore that the dual quark-parton model is capable of giving a satisfactory account of all the principal features of the experimental data shown in fig. 10. In particular the magnitude of the cross section in that range of $\sqrt{q^2}$ where it may plausibly be calculated from the non-diffractive contribution lends support to

the basic notion of the dual quark-parton model which links antiquark contributions in the proton with diffractive effects in deep inelastic electroproduction.

Finally we consider the energy dependence found by Christenson et al. for the total cross section in their mass and momentum aperture. They found that between incident proton energies of 22 GeV and 29.5 GeV it increased monotonically by a factor of 5.

An energy dependence enters our results in several ways. One is the range of integration (5.4). At 22 GeV ω_1 runs from 1 to 1.8. This reduces the value of the contribution from the non-diffractive part in the central $\sqrt{q^2}$ region by a factor of 0.4. However more important for the total cross section is the energy variation of the diffractive contribution, if indeed that provides the large differential cross section at small τ. It will have an explicit energy dependence from (5.9) together with whatever is the appropriate variation of the multiplying function. If we assume that the latter is roughly the same as that we have already calculated for the non-diffractive term the net factor increase between 22 and 29.5 GeV would be about 3.4, which falls a little short of the experimental value.

REFERENCES

[1] P.V.Landshoff, J.C.Polkinghorne and R.D.Short, Nucl. Phys. B19 (1970) 432.
[2] P.V.Landshoff and J.C.Polkinghorne, Nucl. Phys. B28 (1971) 225; Phys. Lett. 34B (1971) 621.
[3] S.D.Drell and T.M.Yan, Phys. Rev. Lett. 24 (1970) 855.
[4] S.D.Drell and T.M.Yan, Phys. Rev. Lett. 25 (1970) 316; preprint SLAC-PUB-808.
[5] R.P.Feynman, Phys. Rev. Lett. 23 (1969) 1415.
[6] P.V.Landshoff and J.C.Polkinghorne, Nucl. Phys. B32 (1971) 541.
[7] P.V.Landshoff, Phys. Lett. 32B (1970) 57.
[8] R.J.Eden, P.V.Landshoff, D.I.Olive and J.C.Polkinghorne, The analytic *S*-matrix (Cambridge University Press, 1966), ch. 3.
[9] J.Christenson, G.Hicks, L.M.Lederman, P.Limon, B.Pope and E.Zavattini, Phys. Rev. Lett. 25 (1970) 1523.
[10] P.V.Landshoff and J.C.Polkinghorne, Nucl. Phys. B19 (1970) 432.
[11] A model for calculating this has been proposed by D.Atkinson and A.P.Contogouris, Bonn preprint.